ORIGINAL PAPER

Mechanical, Thermal and Antimicrobial Properties of Chitosan-Based-Nanocomposite with Potential Applications for Food Packaging

Camila Rodrigues[1] · Josiane Maria Muneron de Mello[2,3] · Francieli Dalcanton[2] ·
Domingos Lusitâneo Pier Macuvele[1,4] · Natan Padoin[1] · Márcio Antônio Fiori[2,3] · Cíntia Soares[1] ·
Humberto Gracher Riella[1]

Abstract

Sodium montmorillonite organically modified by octadecylammonium (Np-Clay) and zinc oxide nanoparticles (Np-ZnO) were incorporated into chitosan (C) matrix in different proportions to evaluate its mechanical properties and antimicrobial activities. The composites were obtained by polymer intercalation method in solution using acetic acid (1% v/v) as solvent. The functional groups, thermic behavior and surface morphology of the chitosan film and of the composites prepared with different percentages of Np-Clay and Np-ZnO were characterized through Fourier transform infrared spectroscopy (FTIR), thermogravimetric analysis (TGA), differential scanning calorimetry (DSC) and scanning electron microscopy (SEM). The results showed that a combined effect of clay and zinc oxide increases significantly the mechanical properties of pure chitosan. FTIR results confirmed good compatibility among functional groups of chitosan, montmorillonite/metallic oxides. The Np-ZnO distribution became more uniform in chitosan films when the Np-clay was incorporated, thus, the Np-Clay compatibilizes the Np-ZnO with the chitosan and the mechanical properties improved and without affecting the antimicrobial activity of the films. The thermal degradation temperature of the chitosan did not change significantly with the addition of Np-Clay, but changes significantly with Np-ZnO addition. In antimicrobial test was found that the chitosan and Np-ZnO showed a synergistic effect against to *Escherichia coli* and *Staphylococcus aureus*. The addition of Np-ZnO and C-Clay in chitosan resulted in enhancement of mechanical and antimicrobial properties, turning this material prospective for food packaging applications.

Graphical Abstract
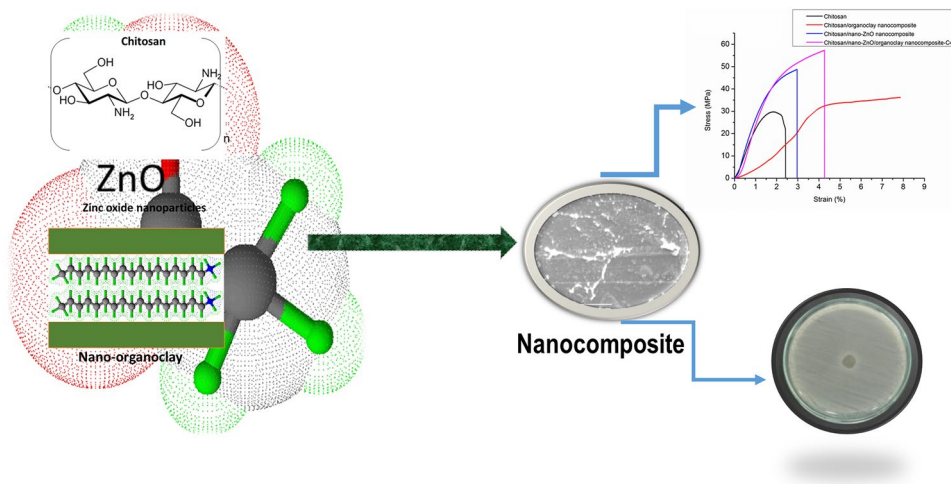
Extended author information available on the last page of the article

Introduction

The food industry, has focused on development of high performance packaging materials with physical, mechanical and antimicrobial properties enhanced and environmentally sustainable. Packaging made from -biopolymers, such as proteins and polysaccharides, are a promising alternative to synthetic polymers [1–3], because they are biodegradable and provide a short life cycle, contributing to sustainable development [4]. Among the biopolymers currently used, chitosan, produced by chitin deacetylation, is as an alternative to be used as active food packaging due to its antimicrobial properties, elasticity, flexibility, biocompatibility and to provide a good oxygen barrier [5–7]. It has a high molecular weight, consisting of pyranose cycles containing at least 50–60% N-acetyl-d-glucosamine and N-glucosamine units and by β $(1 \rightarrow 4)$ glycosidic bonds [6].

Chitosan has application in food, nutrition, biotechnology, materials science, drugs and pharmaceuticals, agriculture and environmental protection, and currently in gene therapy [6, 8–10]. Among many applications, chitosan has attracted interest in food industry to antimicrobial films production and coatings [11]. However, neat chitosan does not fully meet all the criteria of an ideal food packaging, having its mechanical and antimicrobial properties limited. For example, chitosan has a water vapor permeability which may favor the proliferation of pathogenic microorganisms. Additionally, the antimicrobial activity is limited to some types of microorganism. The mechanical, thermal properties of neat chitosan, are poor which depend greatly of composition and chemical structure. For those reasons, the modification of neat chitosan to achieve the high performing material is topic of interest of modern researchers [8]. Several methods have been used to improve the physical, mechanical and antimicrobial properties of chitosan. The addition of micro or nanoparticles [12], the use of crosslinkers and blending with other polymers [13–15] have significantly improved the properties of chitosan. Among the above-mentioned methods, the addition of nanoparticles to the chitosan matrix for the production of nanocomposites has been extensively explored in recent years [12, 16–20]. Chitosan/bacterial cellulose/silver nanoparticles nanocomposite was developed, this hybrid presented enhanced mechanical and antimicrobial properties than neat chitosan [21]. Another study, developed chitosan/gelatin reinforced with silver nanoparticles nanocomposite, and the mechanical properties was improved. Both studies [21, 22], suggest that the enhancement of mechanical is due the best interaction of chitosan and the nanoparticles.

Clay nanoparticles, mainly those belong to the phyllosilicate family of smectite group, being montmorillonite (MMT) the most important and most used to chitosan nanocomposites production. provide an enhancement in the mechanical properties [23–25]. When MMT is modified with alkylamonium salts, the hydrophilic nature can be turned to hydrophilic, enhancing the interaction with polymer matrix consequently the tensile mechanical can be increased [26, 27]. Bentonite clay, composed about 60–95% of montmorillonite is naturally available and their low cost are great advantage to produce bentonite/chitosan nanocomposite [25, 28]. Montmorillonite has no antimicrobial activity, however when modified with essential oils, metal ions and nanoparticles becomes antimicrobial. Therefore, in order to guarantee antimicrobial properties of chitosan films, it is necessary to incorporate an antimicrobial agent [17, 21, 29–31].To improve antimicrobial activity of chitosan, zinc oxide (ZnO) nanoparticles is preferable materials because some desirable properties [32]. Furthermore, ZnO has legal and scientific conditions for commercialization [33]. However, ZnO does not interact effectively with the Chitosan matrix, although it has amine groups capable of partially bind with the empty d orbital of ZnO and the MMT can improve the interfacial characteristic by intercalations/exfoliations [34]. In addition, the leaching of zinc from nanoparticles has recently been reported and this can be relived with addition of bentonite [35].

As described above, there are many studies showing the synthesis of chitosan nanocomposites incorporated with ZnO nanoparticles and some types of clay, to the best of our knowledge, few studies have been found in the literature which evaluate the combined effect of incorporation of nano-ZnO and nano-organophilic bentonite clay on mechanical and antimicrobial properties of Chitosan films for prospective application in food packaging.

On this concept, in this paper were investigated the combination effects of nano-ZnO and nano-organoclay nanoparticles on the mechanical properties and on the antimicrobial activity of the chitosan film applying central composite experimental design.

Experimental Procedures

Materials

Powder chitosan was provided by Purifarma São Paulo (Brazil), the molecular weight of 111.01 kDa and deacetylation degree of 81.9% were determined in our laboratory by Müller [36] adapting the methodology described in the literature

[37]. Briefly this methodology consists in the determination of molar mass by intrinsic viscosity. The flow times were determined using an AVS-350 viscometer of the same capillary brand and correspond to the average of four independent determinations with variation less than 0.1% [36]. Nano-ZnO was supplied by IPEN Laboratory, São Paulo. The Bentonite clay in natura (Np-Clay), with cation exchange capacity of 67 mmol/100 g determined by [38], was supplied by Boane-Mozambique Mine (Africa). The organophilic bentonite, modified by octadecylammonium, used in this work was also produced in our laboratory [39]. *Staphylococcus aureus* (*S. aureus*) and *Escherichia coli* (*E. coli*) were prepared by the Microbiology Laboratory of Universidade Comunitária da Região de Chapecó (UNOCHAPECÓ).

Nanocomposites Preparation

Appropriate amounts of Np-Clay were dispersed in 5 mL of 1% (v/v) acetic acid and kept under stirring for 24 h. Appropriate amounts of Np-ZnO were dispersed in 100 mL of 1% (v/v) acetic acid and kept under stirring for 4 min. In this step, One g of powdered chitosan was added to the zinc oxide solution and stirred for another 4 min to obtain a good dispersion. Then, this dispersion was added in the bentonite dispersion and left under constant stirring for 4 h and sonicated by 2 h. Finally, 20 mL of the final dispersion was added onto petri dishes and kept dry for at least 72 h at room temperature.

Table 1 Central composite design (CCD) parameters obtained for various runs regarding to synthesis of nanocomposites containing Np-Clay and Np-ZnO nanoparticles with different percentages

Experiments	Samples	Np-ZnO (wt%)	Np-Clay (wt%)
1	C1	5.0 (−1)	1.00 (−1)
2	C2	5.0 (−1)	3.00 (1)
3	C3	8.0 (1)	1.00 (−1)
4	C4	8.0 (1)	3.00 (1)
5	C5	4.4 (−α)	2.00 (0)
6	C6	8.6 (α)	2.00 (0)
7	C7	6.5 (0)	0.59 (−α)
8	C8	6.5 (0)	3.40 (α)
9	C9	6.5 (0)	2.00 (0)
10	C9	6.5 (0)	2.00 (0)
Additional experiments for comparison purporse			
11	C	0.0	0.00
12	CClay	0.0	2.00
13	CZnO	6.5	0.00

In other part of table are presented 3 runs (C, CZnO and CClay) for comparison purpose. Percentages used in relation to 1 g of chitosan mass

Nanocomposites samples of chitosan films were obtained containing different percentages of Np-Clay and Np-ZnO, according to experimental design shown in Table 1.

Fourier Transform Infrared (FTIR) Spectra

FTIR spectra were performed in transmission mode by using a software ResolutionsPro version 5.2.0 (Agilent Technologies) in the range of 400–4000 cm^{-1} at a resolution of 4 cm^{-1}. For the test, all composites were submitted in form of films. All samples were submitted to FTIR analysis, however for discussion only one of each samples were chosen. In this part chitosan, chitosan/ZnO nanoparticles, chitosan/organoclay and C9 (best condition from central point experimental design) were analyzed.

Thermogravimetric Analysis (TGA)

Thermal stability of the chitosan film was performed with thermogravimetric analysis in a Netzsch thermogravimetric analyzer, model STA 449 F3 with a temperature program of 25 to 800 °C, at a heating rate of 10 °C/min and flow rate of 80 mL/min in a nitrogen atmosphere. Only one sample of chitosan was evaluated by TGA.

Mechanical Properties

Tensile strength (TS), elongation at break (E) and Young's modulus (YM) of the chitosan film (C) and of the nanocomposites (CClay, CZnO, C1, C2, C3, C4 and C9) were determined with Instron Universal Testing Machine (Model TA.HD.plus Texture Analyzer, Stable Micro Systems). According to ASTM Standard D 882-02 the samples were cut in rectangular specimens (2.54 × 7.5 cm). Initial grip separation was set at 40 mm and cross-head speed was set at 0.01 mm/s. This test was repeated 6 times for each specimen in order to confirm its repeatability, but for statistical purposes were defined just the best three ones (with the lowest standard deviation, in relation to tensile strength).

Differential Scanning Calorimetry (DSC)

DSC measurements were performed with a Perkin-Elmer Jade-DSC. About 7 mg were used and the process was developed in a nitrogen atmosphere at 20 mL/min in three stages: heating from 25 to 400 °C (rate 10 °C/min), followed by cooling to −30 °C (rate 10 °C/min) and reheating up to 400 °C (rate 10 °C/min). The procedure was performed according to ASTM D 3417. The glass transition temperature (Tg) was taken as the inflection point on the DSC thermograph. All nanocomposites without repetitions were analyzed.

Scanning Electron Microscopy (SEM) and Energy Dispersive Spectroscopy (EDS)

Chitosan film (C) and the nanocomposites (CClay, CZnO and C9) were characterized using SEM technique (JEOL JSM-6390LV) joined with EDS technique (NORAN System SIX version 2.0). The films were coated with gold and their surfaces were analyzed with a magnification of 50 times and 5000 times and with voltage of 5 kV and 10 kV. In EDS, a magnification of 150 times and a voltage of 5 kV and 10 kV were used and it was studied one region of the films to observe the elemental distribution of zinc, silicon, oxygen and carbon.

Antibacterial Activity of Np-Clay, Np-ZnO and Composites Films

Antibacterial properties of the Np-Clay, Np-ZnO and of the nanocomposites films were studied using the agar diffusion method and death curve. Gram positive bacteria *Staphylococcus aureus* (American Type Culture Collection—ATCC 25923) and Gram negative bacteria *Escherichia coli* (ATCC 8739) were used for the tests. Bacterial strains were activated in 3.00 mL of Brain Heart Infusion Broth (Himedia) at 37 ± 1 °C for 24 h before starting the tests. 0.10 g of Np-ZnO and Np-Clay and disc-shaped films (1 cm diameter) were poured into Müller-Hinton (Kasvi) agar previously inoculated containing 10^8 CFU/mL of the test bacteria. The result was analyzed by presence or absence of an inhibition halo of microbial growth around the film, whose diameter varies according to the antibacterial diffusion speed and also its sensitivity.

For death curve, films pieces of (2×2 cm) were used, in which samples presented better tensile strength C4 and C9, besides of pure chitosan film, CClay and CZnO composites. The test consists, according to Japanese Standard JIS Z 2801-10, consist in to add in a Petri dish 40µL of a bacterial suspension on the top of each film studied and 1 mL of saline water 0.85% around them, in order to keep the environment humidity favorable to bacterial growth. A sterile glass coverslip was placed on the film to spread the bacteria aliquot throughout the length of the film. Then, the Petri disc (samples) were incubated in chamber at 37 ± 1 °C. The test was performed at times of 0, 6 and 24 h and for each time, serial dilutions were made in a stomacher with a saline solution 0.85%. Then the samples were homogenized and incubated in a chamber in inverted position at 37 ± 1 °C for 24 h. After 24 h the counting of Colony Forming Units per cm^2 (CFU/cm^2) was done, with a colony counter (Quimis brand, model Q295B). The number of viable bacteria per area was calculated according to Eq. 1. The test was performed in triplicate.

$$N = \frac{C * fd * V}{A} \tag{1}$$

where N is the number of viable cells per cm^2, C is the colony count (of 30 to 300 CFU/cm^2), fd is the dilution factor (dimensionless), V is the volume (mL) of saline water 0.85% for sample washing and A is the surface sample area.

Statistical Analysis

The experimental data were obtained with Statistics software version 10 (StatSoft, Inc, USA). Mean comparisons of results regarding mechanical, thermal properties and antibacterial activity were performed applying Tukeys test with 95% of significance. Besides that, the dependent variables from mechanical properties (Tensile strength, strain and Young Modules) and thermal properties (thermal degradation temperature) were treated according to central composite design (CCD) varying the quantities of ZnO nanoparticles and nano organoclay. The choice of this experimental design was due the fact that previous works reported that ZnO and Clay affects the mechanical and antibacterial performance. For CCD the independent variables were codified as $-\alpha, -1, 0, 1, +\alpha$, totalizing 10 experiments, including 4 cube points, 4 axial points and 2 central points. Furthermore, for comparison purpose additional 3 experiments were added. This experiments are regarding to pure chitosan, Chitosan/nanoclay and Chitosan/ZnO nanoparticles. The CCD matrix with additional experiments are presented in Table 1.

The response was modeled by fitting data for quadratic polynomial model with interactions against significant variables (Eq. 2).

$$Y = \beta_0 + \sum_{i=0}^{k} \beta_i x_i + \sum_{i=1}^{k} \sum_{j=1}^{k} \beta_{ij} x_i x_j + \sum_{i=1}^{k} \beta_{ii} x_i^2 + \varepsilon \tag{2}$$

β_0, β_i, β_{ij} and β_{ii} are linear, quadratic and interactions coefficients, respectively. Y is a response (dependent variable), k is the number of factors, j and i are index of factors and ε represent the residual error. Estimated effects was applied to assess the significant and non-significant variables. All statistical interpretations were performed with a confidence 95% using p value as a reference. *Statistica* software version 10, was applied to generated CCD experimental design, and was also used to perform others statistical analysis outside of CCD design.

Results and Discussion

FTIR Analysis

Figure 1 shows the FTIR spectra obtained for the chitosan pure film (C), chitosan/clay (CClay) and chitosan/ZnO (CZnO). To the chitosan pure film the band 3000–3500 cm^{-1} corresponds to the stretching vibration of free hydroxyl and to the symmetric and asymmetric stretching of N–H bonds in amino group of the chitosan molecules [40]. The peaks at 1063 and at 1022 cm^{-1} are associated with the vibrational modes by stretching of the groups -OH, 3′-OH and 5′-OH [20] in chitosan molecules and the peaks at 1639 and 1549 cm^{-1} are associated with the vibrational modes by stretching of C=O group and by scissoring vibration of –NH$_2$ group, respectively [41]. The peaks at 1406 and 1382 cm^{-1} are associated with the vibrational modes of symmetric deformation of CH$_2$ group [42]. The peak at 1323 cm^{-1} corresponding to amide III group, due to deformation combination of NH group and CN stretching vibration and C–O bond present at 1022 cm^{-1} peak. All these functional groups mentioned above are expected to be in the chitosan.

The addition of 2 wt% organo-clay in the chitosan matrix (CClay) provides a peak shift at 3268 cm^{-1} in the pure chitosan spectrum to 3261 cm^{-1}, which is expected from the organo-clay. This peak is associated with NH and OH groups and their shift to lower wave numbers is an indication that –NH$_2$ and –OH groups of the chitosan molecule may be forming lower energy hydrogen bonds with –OH of bentonite [43]. This indicates that organo-clay may be slightly interfering in the intermolecular interactions of chitosan molecules, providing lower energy bonds.

The addition of 6.5% of zinc oxide in the chitosan matrix (CZnO) the peak associated with -OH groups is shifted to a higher wavenumber (3272 cm^{-1}), which is expected from ZnO and indicates that zinc oxide nanoparticles may be
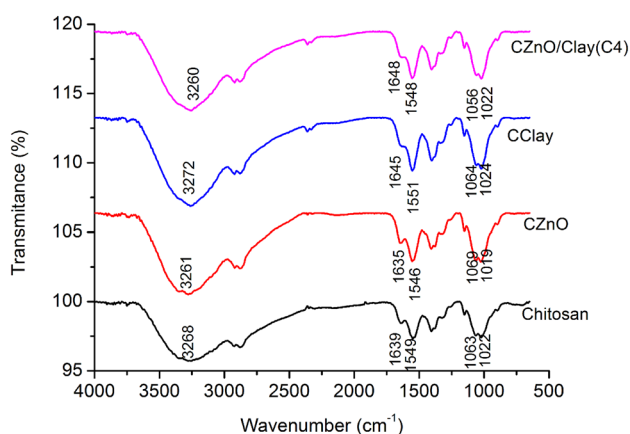
providing intermolecular bonds between chitosan molecules of higher energy. The same behavior is observed with the other spectra peaks associated with the functional groups C=O, –NH$_2$, 3′-OH and 5′-OH corresponding to the peaks (1645 cm^{-1}, 1551 cm^{-1}, 1064 cm^{-1} and 1024 cm^{-1}). These results indicate that zinc oxide nanoparticles provide higher energy vibrational modes, and this phenomenon may be related to the formation of strong hydrogen bonds between ZnO and chitosan molecules.

FTIR results indicate only own peaks of pure chitosan, bentonite nanoparticles or zinc oxide nanoparticles, which prove that there are no significant chemical interactions between their functional groups, just physical interactions. It is also valuable to note that FTIR results corroborate with the ones in the mechanical response.

SEM and EDS Analysis

SEM images of pure chitosan film (C) the nanocomposites films (CClay, CZnO) and the ones with better mechanical response (C4 and C9), with their respective EDS spectra on the surface, are presented in Figs. 2, 3, 4, 5 and 6. Pure chitosan film has a smooth surface with small clusters, probably agglomerates of chitosan molecules, Fig. 2. The EDS spectra in Fig. 2c shows the presence of only carbon, element which composes the pure chitosan without any nanoparticles incorporation. For chitosan films containing organo-clay (CClay) it is possible to observe the presence of clay nanoparticles agglomerates, Fig. 3. The EDS spectra in Fig. 3c shows the presence of the elements Mg, K, Si, Al, O, which correspond to the species found on montmorillonite structure. For the CZnO film a distribution of ZnO nanoparticles in the form of lines (anisotropic) is observed, Fig. 4. The EDS spectra in Fig. 4c indicate the presence of Zn and O, that are attributed to the ZnO nanoparticles structure.

In Figs. 5 and 6a it is clear that the distribution of the zinc oxide nanoparticles is no longer exposed in lines, but it is homogeneously together the clay in the chitosan. This behavior is in agreement with mechanical properties improvement, since the clay compatibilizes the zinc oxide nanoparticles. Figures 5 and 6b show that there are no significant defects among the phases of chitosan, Np-Clay and Np-ZnO and presents less roughness. The EDS spectra in Figs. 5 and 6c show the presence of C, Zn, Si, N and O, which represents the incorporation of both clay and ZnO nanoparticles into chitosan.

TGA Analysis

The thermal stability of the pure chitosan film was evaluated through thermogravimetry analysis (TGA) and its respective DTG curve, presented in Fig. 7. In the thermogram the first
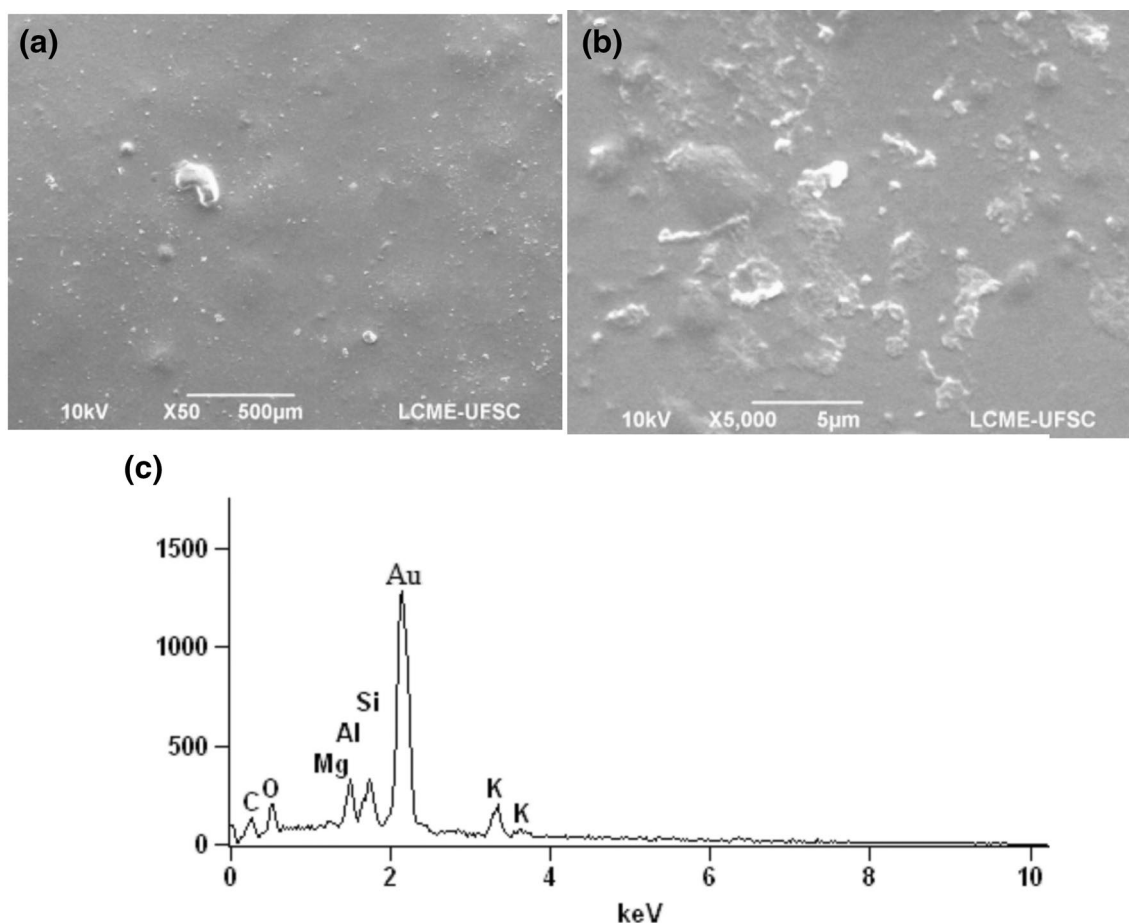

Fig. 1 FTIR spectra obtained for the pure chitosan film (C) and its nanocomposites
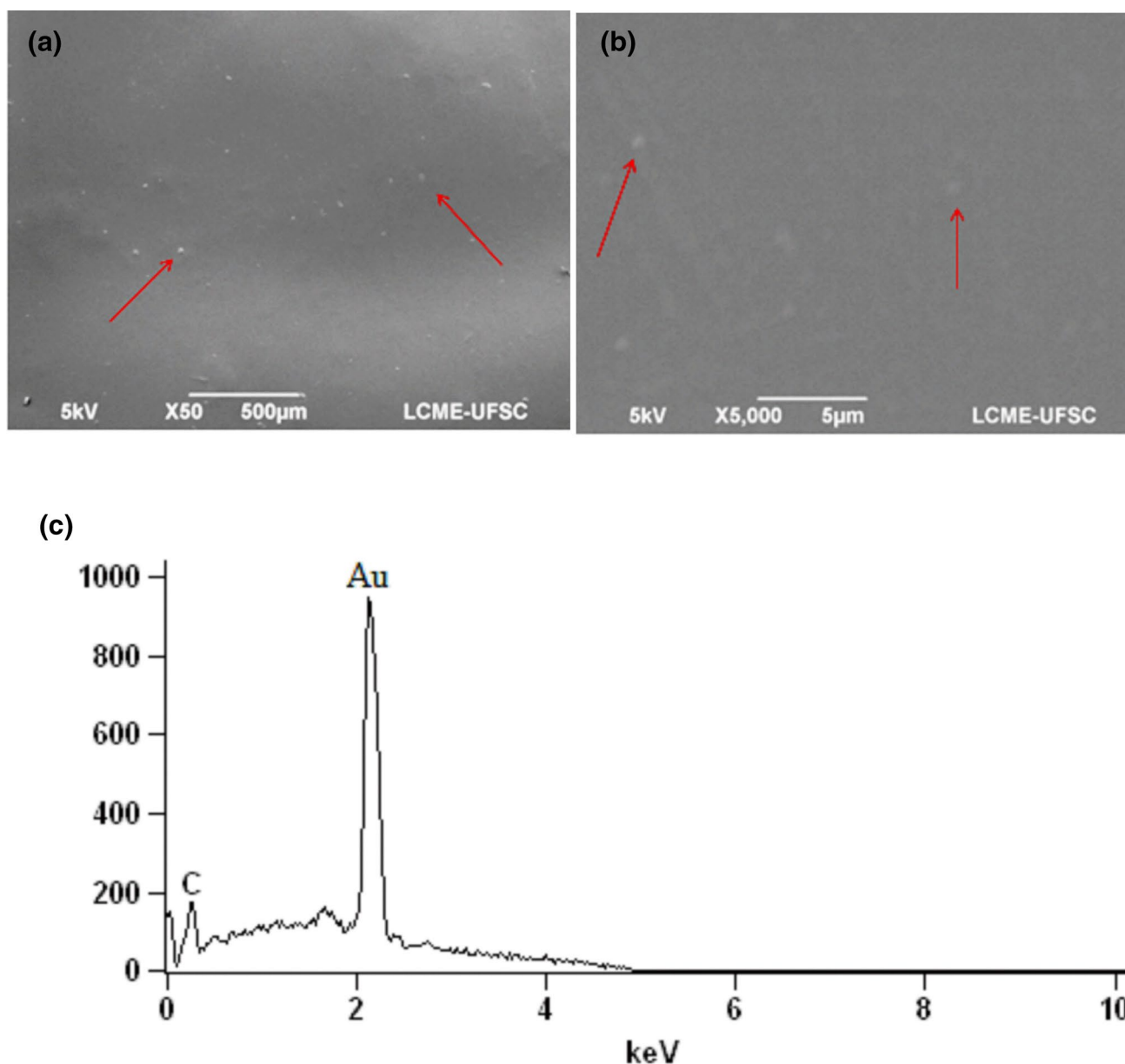
Fig. 2 SEM images from the surface of Chitosan in the magnification of **a** ×50; **b** ×5000 and **c** EDS spectra

thermal stage refers to water molecules release bound mainly in amino and hydroxyl groups of the chitosan. The release starts at 23.01 °C and goes up to 162.07 °C and represents 17.38% of the total chitosan mass. The second thermal stage corresponds to organic material loss and thermal degradation of chitosan molecules. This stage starts at 162.07 °C and ends at 792.78 °C, corresponding to a 70.73% mass loss. After 400 °C the remaining total mass is around 30% and it corresponds to carbon (ashes) as product of thermal degradation of chitosan. It is also important to mention that the thermal stability of the chitosan is affected depending on intrinsic factors (degree of deacetylation, molecular weight, purity, and moisture level) and extrinsic ones (environmental storage conditions, thermal processing, and processing involving acidic dissolution) which are acknowledged as crucial parameters [44].

DSC Analysis

The differential scanning calorimetric analysis thermograms for the pure chitosan film (C), chitosan/organo-clay (CClay) and chitosan/ZnO (CZnO) nanocomposites are shown in Fig. 7. The thermogram shows a transition region starting at 23.01 °C and goes up to 162.07 °C correspondent to the dehydration of the chitosan. Close to 300 °C the thermogram
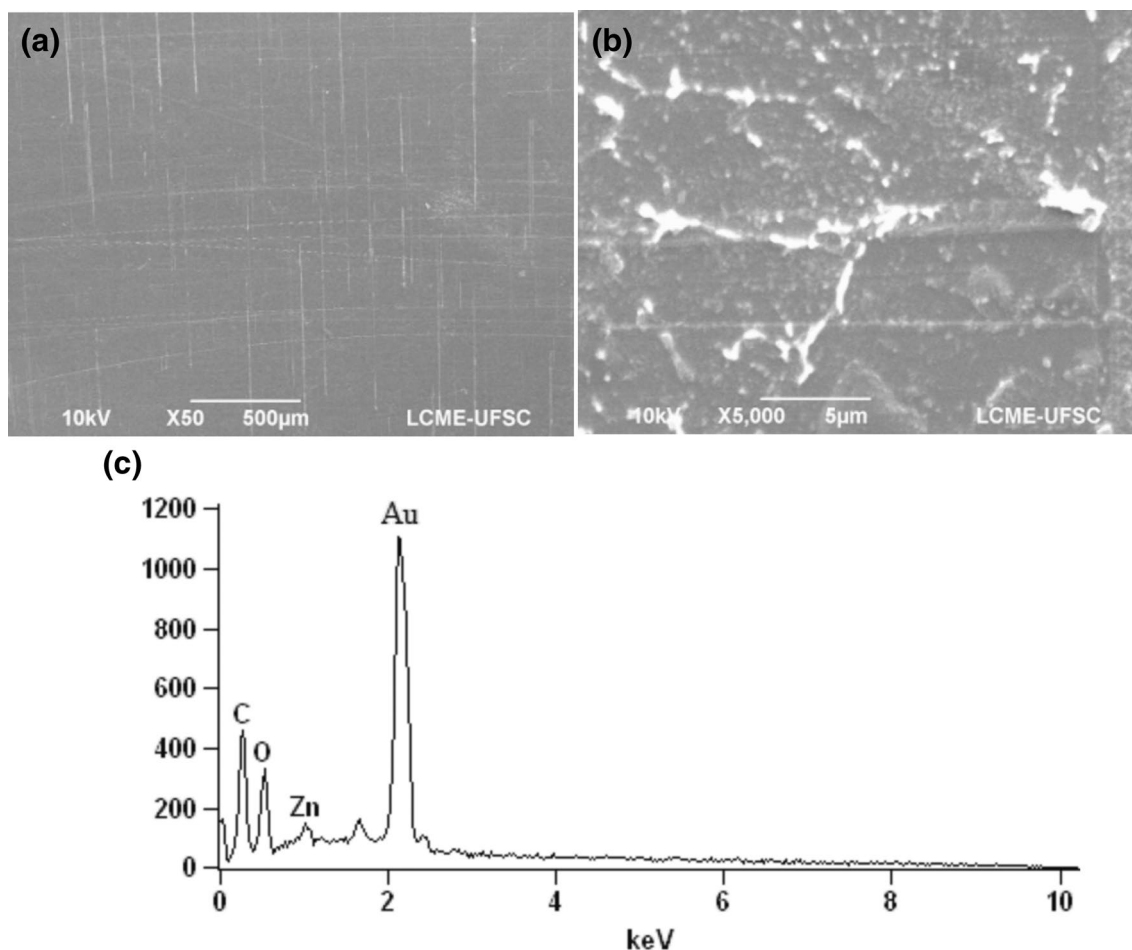
Fig. 3 SEM images from the surface of CClay in the magnification of **a** ×50; **b** ×5000 and **c** EDS spectra

shows a transition correspondent to the thermal degradation of the chitosan. The dehydration temperature, dehydration enthalpy, degradation temperature, degradation enthalpy and glass transition temperature obtained for pure chitosan film and for the composites containing different percentages of Np-Clay and Np-ZnO are presented in Table 2.

The thermograms show two characteristic peaks in the heating condition, one endothermic and other exothermic. The endothermic peaks occur in temperatures around 70–85 °C and are attributed to the dehydration process of chitosan molecules and nanocomposites. In this process occurs the water release bound to hydrophilic groups of chitosan molecules [45]. The addition of Np-Clay and Np-ZnO do not change significantly the dehydration temperature of the chitosan molecules. The exothermic peaks in the range of 268–292 °C are attributed to the structural degradation of chitosan, a process that is usually related to the thermal degradation of glucosamine units present in its molecular structure [46]. The thermal degradation temperature of the chitosan is 289 °C and with Np-Clay incorporation it does not undergo significant modifications.

However, with Np-ZnO incorporation the thermal degradation temperature of chitosan is 269 °C, a significant reduction. The reduction of thermal degradation temperature of chitosan may favor hydrolysis reactions of the chitosan molecules by the zinc oxide nanoparticles [47]. As well as, at higher concentrations of nanoparticles (> 4–5 wt%) can form aggregates and thus the effective area of nanoparticles in contact with polymer macromolecular is lower. In this case microcomposites can be formed instead of nanocomposites and thus the protective effect of nanoparticles becomes lower [48].

The glass transition temperature (Tg) for the pure chitosan film is around 197 °C, a value close to the one obtained by [49], which report a chitosan Tg of 203 °C and indicates a flexible structure. The addition of Np-Clay and Np-ZnO did not change significantly the glass transition temperature of chitosan. The thermogram of the pure chitosan film and of the nanocomposites did not show transition peaks associated with melting. This can be explained by the fact that most polysaccharides do not melt but undergo thermal degradation at relatively low temperatures [50]. As a consequence,

Fig. 4 SEM images from the surface of CZnO in the magnification of **a** × 50; **b** × 5000 and **c** EDS spectra

are not observed peaks related to melting in heating process and of crystallization in a cooling process.

Table 3, shows the estimated effects table regarding to thermal degradation temperature as function of percentage of Np-ZnO and clay in experimental design. According to the Table 3, only the percentage of Np-ZnO causes statistically significant effects on the nanocomposites and only in thermal degradation temperature (Ttd). The increases of the zinc oxide nanoparticles decrease the degradation temperature of the chitosan molecules. According to [51] the ZnO is a semiconductor and is capable of generating free oxygen and oxygen vacancies in the polymeric structures, induced by thermal stimulation. Oxygen vacancies are able to absorb electrons and generate active catalytic conditions in the regions where ZnO molecules are positioned. The free oxygen in the polymer structure favors the formation of peroxide radicals that accelerate the oxidation process of the chitosan chains and their thermal degradation with hydrolysis reactions of the polymer [47]. Increasing the percentage of zinc oxide nanoparticles in the composite provides an increase in the amount of oxygen vacancies and peroxide

radicals formation and, as a consequence, the thermal degradation of chitosan molecules happens at lower temperatures.

The statistical results show that a linear correlation model between the percentage of zinc oxide nanoparticles and degradation temperature is appropriate. The value of 0.94 for coefficient of determination (R^2) shows a satisfactory linear fit. As only the percentage of zinc oxide nanoparticles is significant for degradation temperature of the composite it is possible to propose a linear statistical model with only one variable. Equation 3 correlates the effect of thermal degradation temperature (ETtd) with the percentage of zinc oxide nanoparticles (Np-ZnO).

$$ETtd(Np\text{-}ZnO) = 270(\pm0.45) - 2.06(\pm0.22)Np\text{-}ZnO \quad (3)$$

In practice, the equation is important because it represents a method to degradation temperature estimation of the composite as function of Np-ZnO percentage in the development and production of chitosan based nanocomposites. In Fig. 8 the response surface (A) and contours figure (B) can be observed, showing the linear dependence
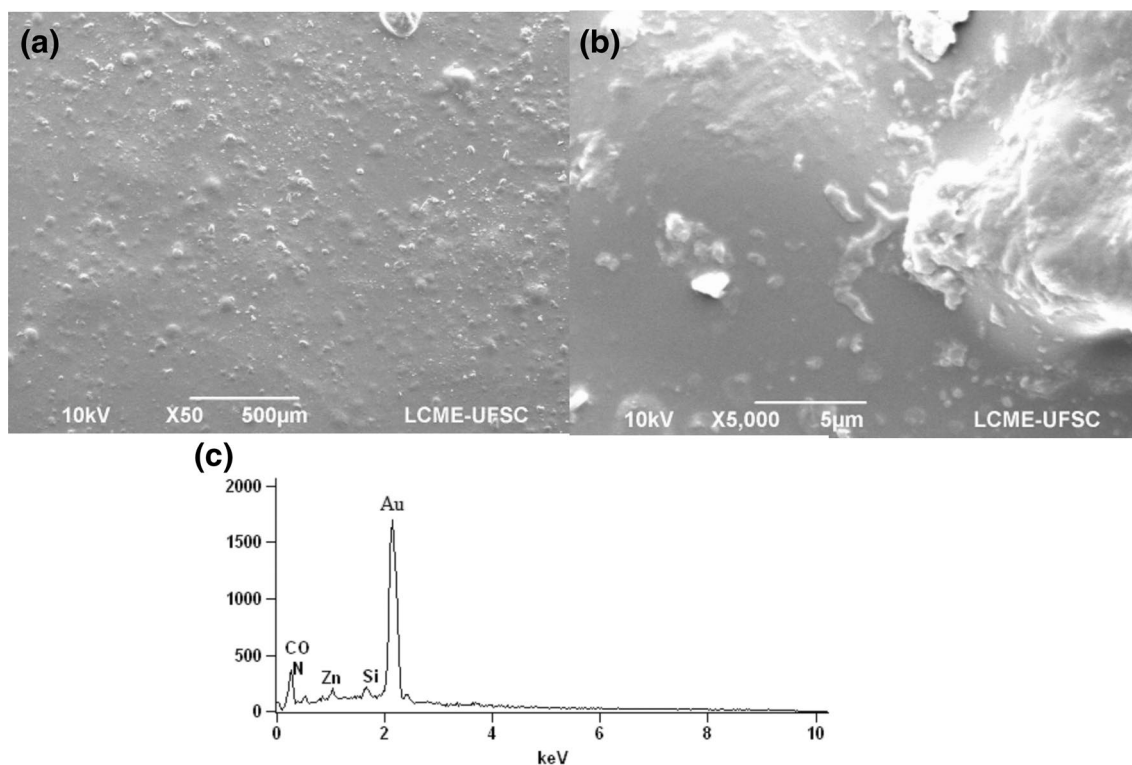
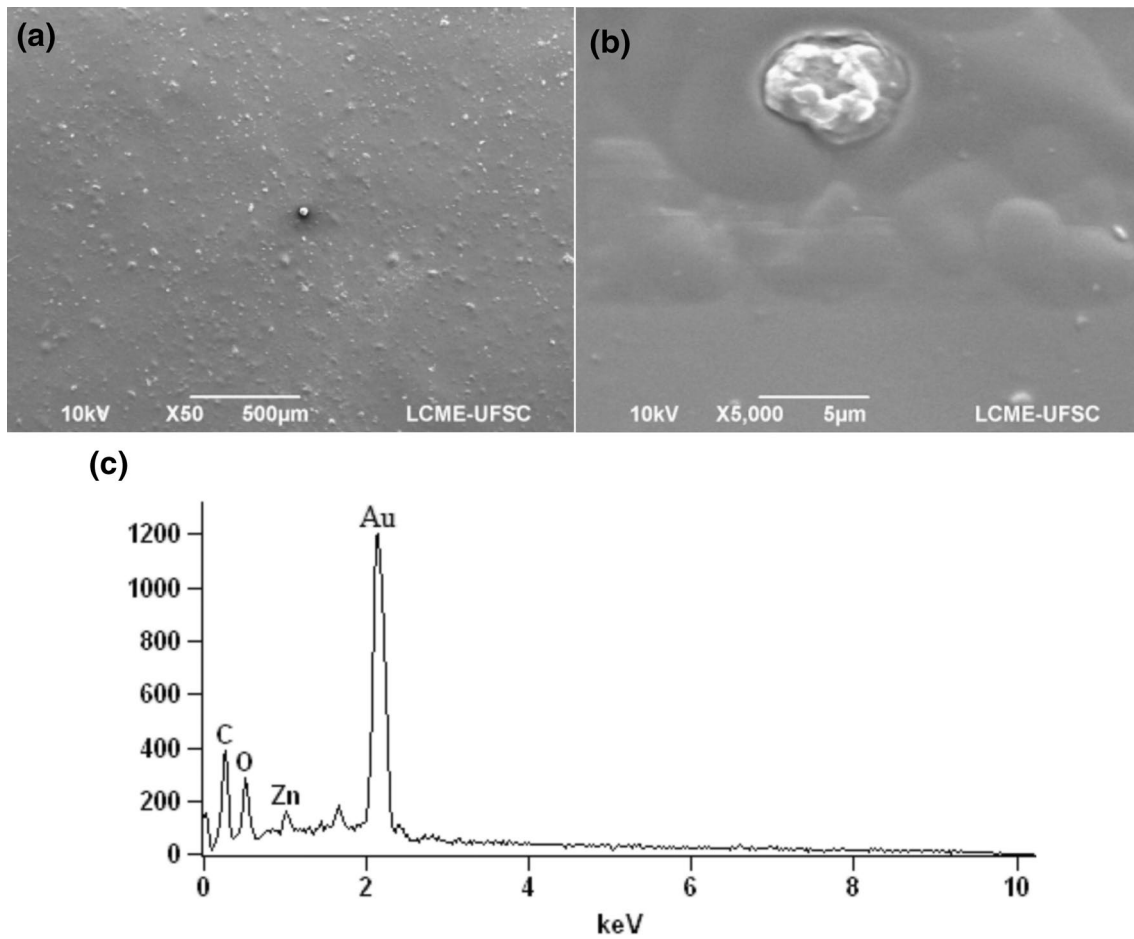**Fig. 5** SEM images from the surface of C4 in the magnification of **a** ×50; **b** ×5000 and **c** EDS spectra

of Np-ZnO concentration as function of thermal degradation temperature. The best regions were observed at levels $(-1, -1)$, $(-\alpha, 0)$ and $(-1, 1)$ corresponding to samples C5 (2% Clay + 4.4% ZnO), C2 (3% Clay + 5% ZnO) and C1 (1% Clay + 5% ZnO). It is seen in the graphical representations that the behavior and magnitude for degradation temperature effect are not modified significantly with clay concentration variations. The ZnO percentage of 4,4 in chitosan reduces the thermal degradation temperature in 3,4%. Consequently, with the increase of the other ZnO percentages (5,0; 6,5; 8,0 and 8,6) the thermal degradation gets more and more high (3,82; 4,96; 6,11 and 6,45%), respectively. This reduction shows to be very expressive and it's evident that the thermal stability of the nanocomposites is damaged.

Mechanical Properties

The results regarding of tensile mechanical properties are presented in Figs. 9, 10, 11 and 12. Figure 12, shows the typical stress–strain mechanical response (tensile strength × strain) of the pure chitosan film (C), nanocomposites CCla, CZnO and C4. Table 4, show values for maximum tensile strength, elongation at break and Young's modulus obtained with the pure chitosan film and different percentages of Np-Clay and Np-ZnO. The results showed

that, all the nanocomposites presented high values of tensile strength than pure chitosan. This results are in agreement with previous works [17, 26]. Interestingly, the simultaneous addition of ZnO nanoparticles and nanoclay increased the tensile strength, suggesting an improvement of interfacial characteristics of resulted nanocomposite [27]. An enhancement of homogeneity in chitosan matrix was observed in SEM micrographs and emphasized with FTIR analysis that showed an interaction with functional groups.

To understand how the ZnO nanoparticles and nanoclay affect the tensile mechanical an experimental design was performed. Matrix of estimated effects for for tensile strength as a response variable is presented in Table 5, in Table 6 for elongation at break and in Table 7 for Young's modulus. According to the experimental design results tensile strength is affected significantly only by the concentration of zinc oxide nanoparticles and with positive effect. The average effect of Np-ZnO addition is an increase of (15.60 ± 2.66) in the value of maximum tension. Chitosan molecules, have a large number of cyclic chain structures that favor the formation of hydrogen bonds with –OH and –NH$_2$ groups. These bonds make the rotation difficult and also the other chain molecular movements and are responsible for the mechanical properties of the chitosan film. ZnO nanoparticles act as interface coupling agents of chitosan molecules and provide intermolecular bonds

Fig. 6 SEM images from the surface of C9 in the magnification of **a** ×50; **b** ×5000 and **c** EDS spectra
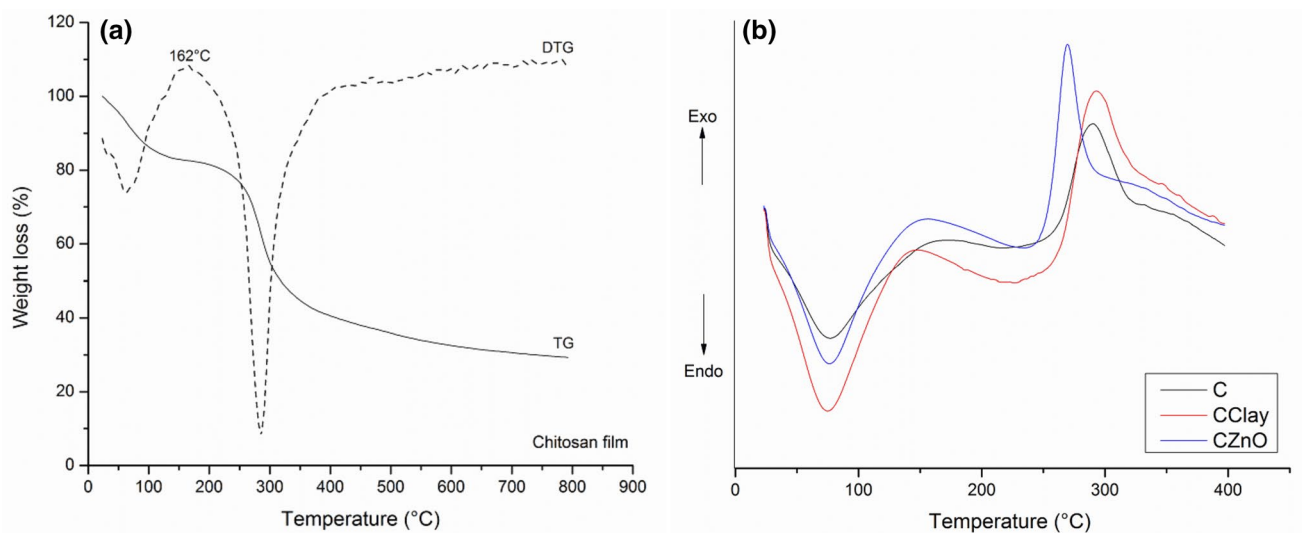
Fig. 7 Thermograms: **a** TG and its derivative DTG to the pure chitosan film, and **b** DSC for pure chitosan film (C), chitosan/clay (CClay) and chitosan/ZnO (CZnO) nanocomposites

Table 2 Values for dehydration temperature, dehydration enthalpy, degradation temperature, degradation enthalpy and glass transition temperature for pure chitosan film and nanocomposites containing different percentages of Np-Clay and Np-ZnO

Samples	Clay (wt%)	ZnO (wt%)	Td (°C)	ΔHd (J/g)	Ttd (°C)	ΔHtd (J/g)	Tg (°C)	R²
C	0.00	0.0	76	165.50	289	144.48	197.49	0.95
CClay	2.00	0.0	74	239.36	292	237.30	181.44	0.90
CZnO	0.00	6.5	76	209.51	269	112.50	196.45	0.90
C1	1.00	5.0	75	317.81	271	197.95	197.28	0.86
C2	3.00	5.0	78	248.03	273	147.23	189.72	0.86
C3	1.00	8.0	85	310.85	268	153.53	194.31	0.90
C4	3.00	8.0	79	275.47	268	151.57	190.95	0.92
C5	2.00	4.4	70	205.12	274	118.02	187.21	0.88
C6	2.00	8.6	76	190.32	268	138.75	206.84	0.89
C7	0.59	6.5	79	316.80	270	156.40	193.67	0.90
C8	3.40	6.5	85	298.36	270	194.70	203.30	0.87
C9	2.00	6.5	82	272.49	270	157.89	186.81	0.84

Experimental conditions defined according to a central composite design

Td dehydration temperature, *ΔHd* dehydration enthalpy, *Ttd* thermal degradation temperature, *ΔHtd* thermal degradation enthalpy, *Tg* glass transition temperature, R^2 correlation coefficient corresponding to the values of ΔHd and ΔHtd

Table 3 Matrix of effect estimates for degradation temperature results

|	Effect Estimates; Var.: Ttd (°C); R-sqr = 0.94603							
	Effect	Std Err	t(5)	p	−95%	95%	Coeff	Std. Err. Coeff
Mean	270.00	0.45	599.34	0.00	268.84	271.15	270.00	0.45*
ZnO (L)	−4.12	0.45	−9.14	0.00	−5.27	−2.96	−2.06	0.22*
ZnO (Q)	0.75	0.59	1.25	0.26	-0.78	2.28	0.37	0.29
Clay (L)	0.50	0.45	1.10	0.31	−0.65	1.65	0.25	0.22
Clay (Q)	−0.25	0.59	−0.41	0.69	−1.78	1.28	−0.12	0.29

*Represents the significant effect

L linear model, *Q* quadratic model
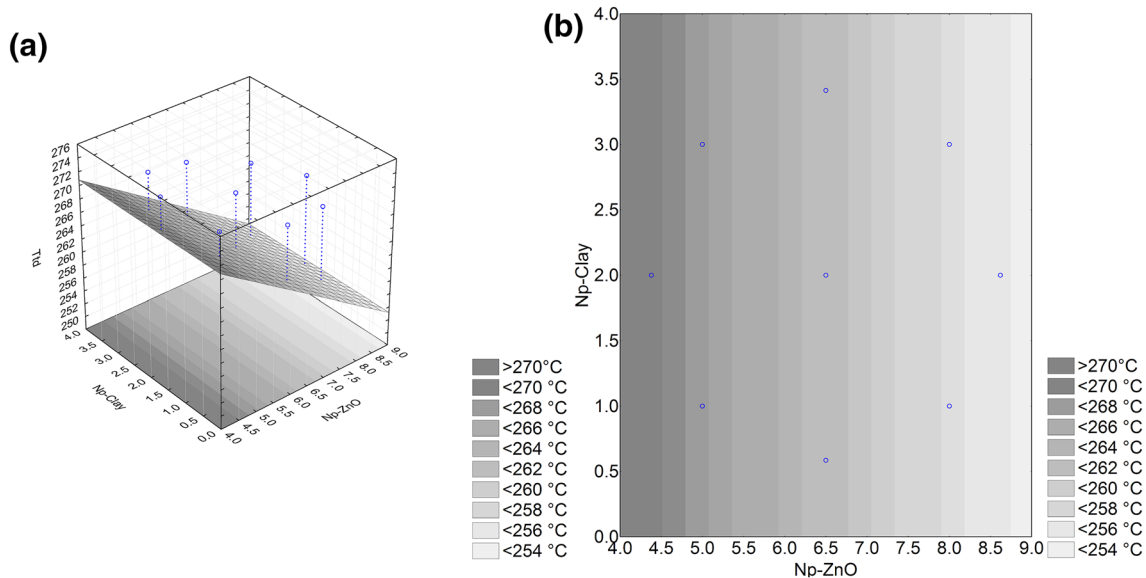
Fig. 8 Response surface (**a**) and contours (**b**) to degradation temperature values
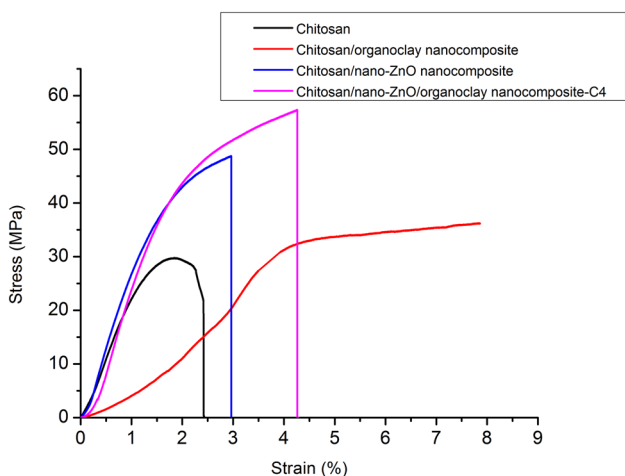
**Fig. 9** Representative tensile strength × strain test for pure chitosan film and the nanocomposites

of higher bond energy, which favors the rotation motions of the molecular chains and increase the tensile strength of the films constituted by the nanocomposite [20]. Zinc oxide nanoparticles are dispersed homogeneously in the chitosan matrix that prevents molecular coagulation, as result of fewer interface defects are obtained in the films containing Np-ZnO and tensile strength property is improved [19]. Although of the non-significant effect of nanoclay on the tensile strength, this play an important role as compatibilizer of chitosan and ZnO nanoparticles. SEM micrographs of nanocomposite with nanoclay presented an homogenous surface than nanocomposites without nanoclay. Also, the FTIR analysis suggested a type of interactions with functional groups. Similar results were obtained in other research [52].

Furthermore, the statistical results show that a linear correlation model between the percentage of zinc oxide nanoparticles and maximum tensile strength is appropriate. The value of 0.77 for the correlation coefficient (R^2) shows a linear fit. As only the percentage zinc oxide nanoparticles is significant for maximum tensile strength of the composite it is possible to propose a linear statistical model with only one variable. Equation 4 correlates the effect of the maximum tensile strength (Et) with the percentage of zinc oxide nanoparticles (Np-ZnO).

$$Et(Np\text{-}ZnO) = 30.48(\pm1.19) + 7.79(\pm1.33)Np\text{-}ZnO \quad (4)$$

In practice, the equation is important because it presents a method to the maximum tensile strength estimation of the nanocomposite as function of Np-ZnO percentage in the development and production of the nanocomposites. In Fig. 10 the response surface (A) and contours (B) can be observed, showing the linear dependence of ZnO concentration as a function of tensile strength. The best values were observed at levels (+1, +1) and (0, 0) corresponding to samples C4 (3% Clay + 8% ZnO) and C9 (2% Clay + 6.5% ZnO). It is seen in the graphical representations that the behavior and magnitude for tensile strength effect are not modified significantly with clay concentration variations.

For elongation at break, the percentage of ZnO nanoparticles and the percentage of clay nanoparticles are statistically significant factors. Both have a positive effect on the elongation capacity of the films until rupture. With effect of (0.92 ± 0.12) for Np-ZnO percentage and of (0.31 ± 0.12) for Np-Clay percentage. The presence of zinc oxide nanoparticles in the chitosan matrix reduces the amount of interface defects and favors the molecular movement of chitosan
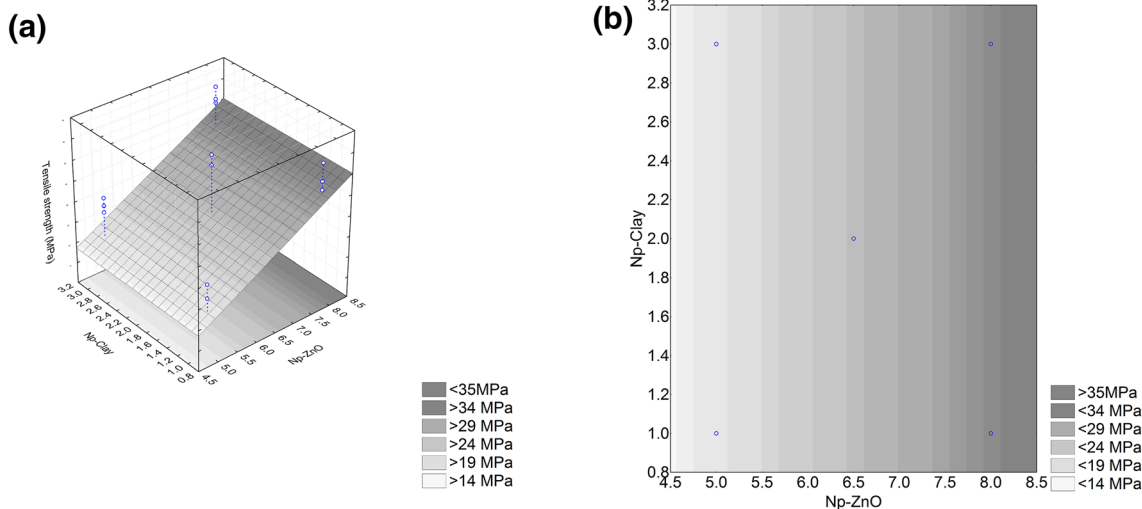
Fig. 10 Response surface (**a**) and contours (**b**) to tensile strength values

(a)

(b)
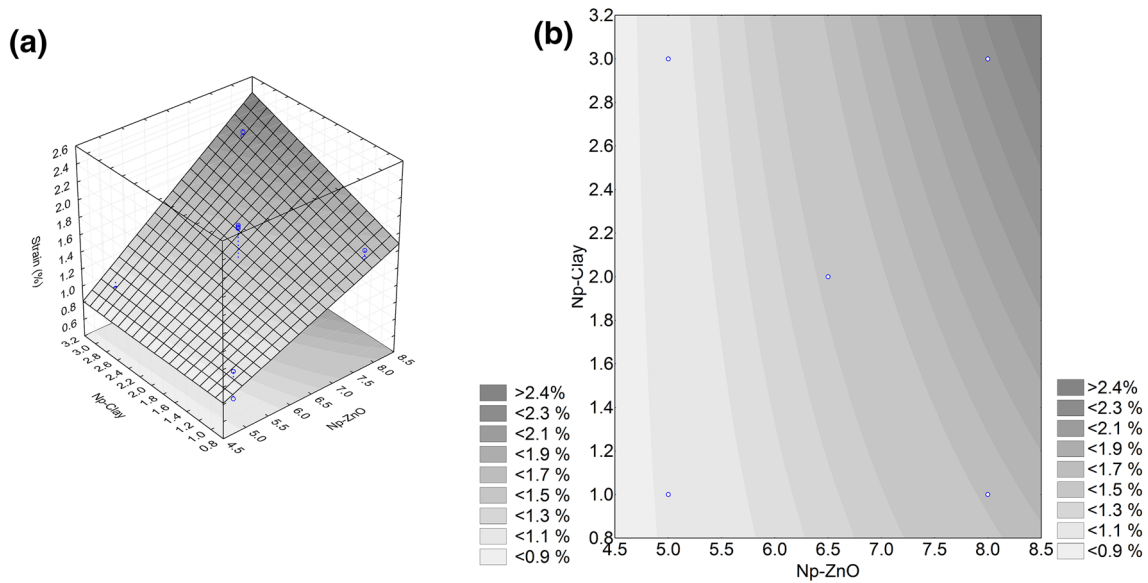
Fig. 11 Response surface (**a**) and contours (**b**) to elongation values

(a)

(b)
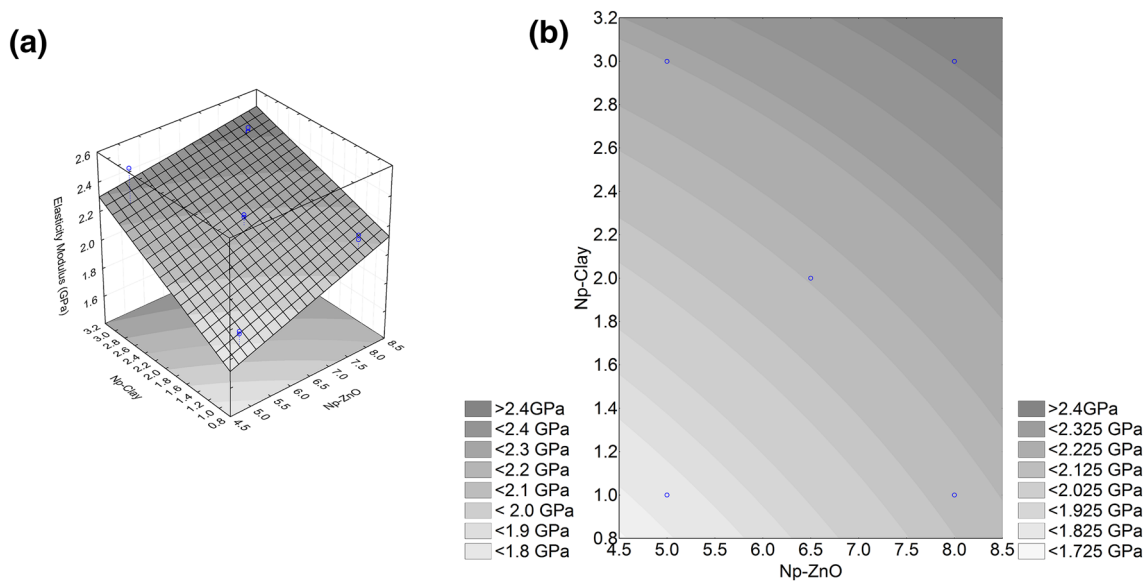
Fig. 12 Response surface (**a**) and contours (**b**) to Young's modulus values

molecules. In this way, the deformation capacity of polymer matrix on a field of tension deformation is favored, allowing the films have a bigger elongation capacity until their rupture. On the other hand, the incorporation of clay nanoparticles favors a good dispersion of zinc oxide nanoparticles along the chitosan matrix, thus permitting the interface area increase and contributing to the effect of Np-ZnO coupling agent. Similar research used organophilic clay nanoparticles to improve the dispersion of erucamide in the polymer

matrix. The authors obtained better mechanical performances and better compatibility between erucamide and the polymer matrix with the increase of organophilic clay nanoparticles percentage [52].

The statistical results show that a linear correlation model between the percentage of clay nanoparticles and zinc oxide nanoparticles and the elongation is appropriate. The value of 0.84 for the coefficient of determination (R^2) shows a satisfactory linear fit. As the percentage of

Table 4 Maximum tensile strength, elongation and Young's modulus values obtained for pure chitosan film and containing different percentages of Np-Clay and Np-ZnO

Samples	Clay (wt%)	ZnO (wt%)	TS (MPa)	E (%)	YM (GPa)
C	0	0.0	33.68±2.28	3.45±0.27	2.040±0.15
CClay	2	0.0	22.34±1.75	1.54±0.07	1.750±0.06
CZnO	0	6.5	30.49±1.17	1.48±0.01	2.190±0.02
C1	1	5.0	18.27±2.60	0.84±0.14	1.800±0.08
C2	3	5.0	23.77±1.20	0.92±0.03	2.260±0.15
C3	1	8.0	34.37±2.40	1.54±0.06	2.090±0.05
C4	3	8.0	38.86±1.49	2.08±0.05	2.410±0.01
C9	2	6.5	37.08±1.10	1.78±0.01	2.220±0.01

Experimental conditions defined according to a factorial design

TS tensile strength, *E* elongation, *YM* young's modulus

Table 5 Matrix of effect estimates for tensile strength results

	Effect Estimates; Var.:Tensile strength (MPa); R-sqr=0.77603							
	Effect	Std Err	t(11)	p	−95%	95%	Coeff	Std. Err. Coeff
Mean	30.47	1.18	25.67	0.00	27.85	33.08	30.47	1.18*
(1) ZnO	15.59	2.65	5.87	0.00	9.75	21.43	7.79	1.32*
(2) Clay	4.99	2.65	1.88	0.08	−0.84	10.83	2.49	1.33
1 by 2	−0.50	2.65	−0.19	0.85	−6.34	5.33	−0.25	1.33

*Represents the significant effect

Table 6 Matrix of effect estimates for elongation at break results

	Effect Estimates; Var.:Elongation at break (%); R-sqr=0.84551							
	Effect	Std Err	t(11)	p	−95%	95%	Coeff	Std. Err. Coeff
Mean	1.43	0.05	24.82	0.00	1.30	1.55	1.43	0.05*
(1) ZnO	0.92	0.12	7.15	0.00	0.63	1.20	0.46	0.06*
(2) Clay	0.31	0.12	2.40	0.03	0.02	0.59	0.15	0.06*
1 by 2	0.23	0.12	1.78	0.10	−0.05	0.51	0.11	0.06

*Represents the significant effect

Table 7 Matrix of effect estimates for Young's modulus results

	Effect Estimates; Var.:Elongation at break (%); R-sqr=0.84551							
	Effect	Std Err	t(11)	p	−95%	95%	Coeff.	Std. Err. Coeff.
Mean	2.15	0.02	78.11	0.00	2.09	2.21	2.15	0.02*
(1) ZnO	0.22	0.06	3.59	0.00	0.08	0.35	0.11	0.03*
(2) Clay	0.39	0.06	6.35	0.00	0.25	0.52	0.19	0.03*
1 by 2	−0.06	0.06	−1.12	0.28	−0.20	0.06	−0.03	0.03

*Represents the significant effect

clay nanoparticles and zinc oxide nanoparticles are significant for the elongation of the nanocomposite it is possible to propose a linear statistical model with two variables. Equation 5 correlates the effect of the elongation (Ee) with the percentage of clay nanoparticles (Np-Clay) and zinc oxide nanoparticles (Np-ZnO).

$$Ee(\text{Np-ZnO, Np-Clay}) = 1.43(\pm 0.057)$$
$$+ 0.47(\pm 0.064)\text{Np-ZnO}$$
$$+ 0.15(\pm 0.064)\text{Np-Clay} \quad (5)$$

In practice, the equation is important because it presents a method to the elongation estimation of the composite as function of Np-Clay and Np-ZnO percentage in the development and production of nanocomposites. In Fig. 11 the response surface (A) and contours (B) can be observed, showing the linear dependence of clay and ZnO concentration as a function of elongation at break. The best region was observed at level $(+1, +1)$ corresponding to sample C4 (3% Clay + 8% ZnO).

The effect of zinc oxide nanoparticles and clay nanoparticles addition on Young's modulus values is similar. With higher percentage of ZnO nanoparticles and clay nanoparticles occur the increase of films stiffness obtained with the nanocomposites. Increasing the percentage of zinc oxide nanoparticles from 5 to 8% has a positive mean effect on Young's modulus of (0.23 ± 0.06), while the percentage increase from 1 to 3% of clay nanoparticles has a positive mean effect of (0.39 ± 0.06). The statistical results also show that a linear correlation model between the clay nanoparticles and zinc oxide nanoparticles percentage and the Young's modulus is appropriate. The value of 0.84 for the correlation coefficient (R^2) shows a satisfactory linear fit. As the percentage of clay nanoparticles and zinc oxide nanoparticles are significant for Young's modulus of the composite it is possible to propose a linear statistical model with two variables. Equation 6 correlates the effect of the modulus (Em) with the percentage of clay nanoparticles (Np-Clay) and zinc oxide nanoparticles (Np-ZnO).

$$Em(\text{Np-ZnO, Np-Clay}) = 2.15(\pm 0.027)$$
$$+ 0.11(\pm 0.03)\text{Np-ZnO}$$
$$+ 0.19(\pm 0.03)\text{Np-Clay} \quad (6)$$

In practice, the equation is important because it presents a method to Young's modulus estimation of the composite as function of Np-Clay and Np-ZnO percentage in the development and production of nanocomposites. In Fig. 12 the response surface (A) and contours (B) can be observed, showing the linear dependence of clay and ZnO concentration as a function of Young's modulus. The best region was observed at level $(+1, +1)$ corresponding to sample C4 (3% Clay + 8% ZnO).

Summary, the addition of ZnO and clay nanoparticles improved the tensile mechanical properties of nanocomposites. Importantly, the tensile strength was significantly improved by ZnO nanoparticles, but according to SEM, FTIR analysis the nanoclay improve the interfacial characteristics enhancing the interactions between phases. In addition, elongation and Young modulus, are signicantly affected by both fillers added in chitosan matrix.

Antibacterial Activity

Table 8 shows the results of antimicrobial tests for organophilic clay nanoparticles and zinc oxide nanoparticles. It is also presented the results for pure chitosan film (C) and the nanocomposites films (CClay, CZnO) and the ones with better mechanical response (C4 and C9). The plates' images of agar diffusion test against *S. aureus* and *E. coli* bacteria for organophilic clay nanoparticles and zinc oxide nanoparticles are shown in Fig. 13. As seen in Fig. 13 a bacteriostatic effect for both bacteria was observed only to Np-ZnO, since an inhibition halo of microbial growth was formed. However, to Np-Clay no inhibition halo was identified.

In Figs. 14 and 15 are presented the plates images of agar diffusion test on solid medium for the film samples against *S. aureus* and *E. coli* bacteria. For chitosan pure film (control) (Fig. 14) the inhibition zone was difficult to visualize for both bacteria, as it does not present a well-defined halo, showing diffuse towards the middle. Although this test does not state that the studied

Table 8 Antimicrobial tests results for Np-Clay, Np-ZnO, pure chitosan film (C) and for the nanocomposites films (CClay, CZnO, C4 and C9)

| Samples	Amounts		Agar diffusion test		Death curve test					
			Inhibition halo mean values (mm)		*S. aureus*		*E. coli*		% reduction (24 h)	
	Clay (wt%)	ZnO (wt%)	*E. coli*	*S. aureus*	0 h	24 h	0 h	24 h	*S. aureus*	*E. coli*
Np-Clay	–	–	0.0 ± 0.0	0.0 ± 0.0	–	–	–	–	–	–
Np-ZnO	–	–	30.0 ± 0.6	80.0 ± 10.0	–	–	–	–	–	–
C	0	0.0	Diffuse	Diffuse	1.00 ± 0.183	0.010 ± 0.007	1.000 ± 0.142	0.000 ± 0.000	99.5	100.0
CClay	2	0.0	0.0 ± 0.0	0.0 ± 0.0	1.000 ± 0.194	0.000 ± 0.000	1.000 ± 0.217	0.000 ± 0.000	100.0	100.0
CZnO	0	6.5	10.0 ± 0.6	20.0 ± 0.5	1.000 ± 0.097	0.000 ± 0.000	1.000 ± 0.253	0.000 ± 0.000	100.0	100.0
C4	3	8.0	10.0 ± 0.5	10.0 ± 0.5	1.000 ± 0.657	0.000 ± 0.000	1.000 ± 0.247	0.210 ± 0.214	100.0	95.4
C9	2	6.5	20.0 ± 0.6	30.0 ± 0.6	1.000 ± 0.553	0.000 ± 0.000	1.000 ± 0.317	0.070 ± 0.060	100.0	96.9
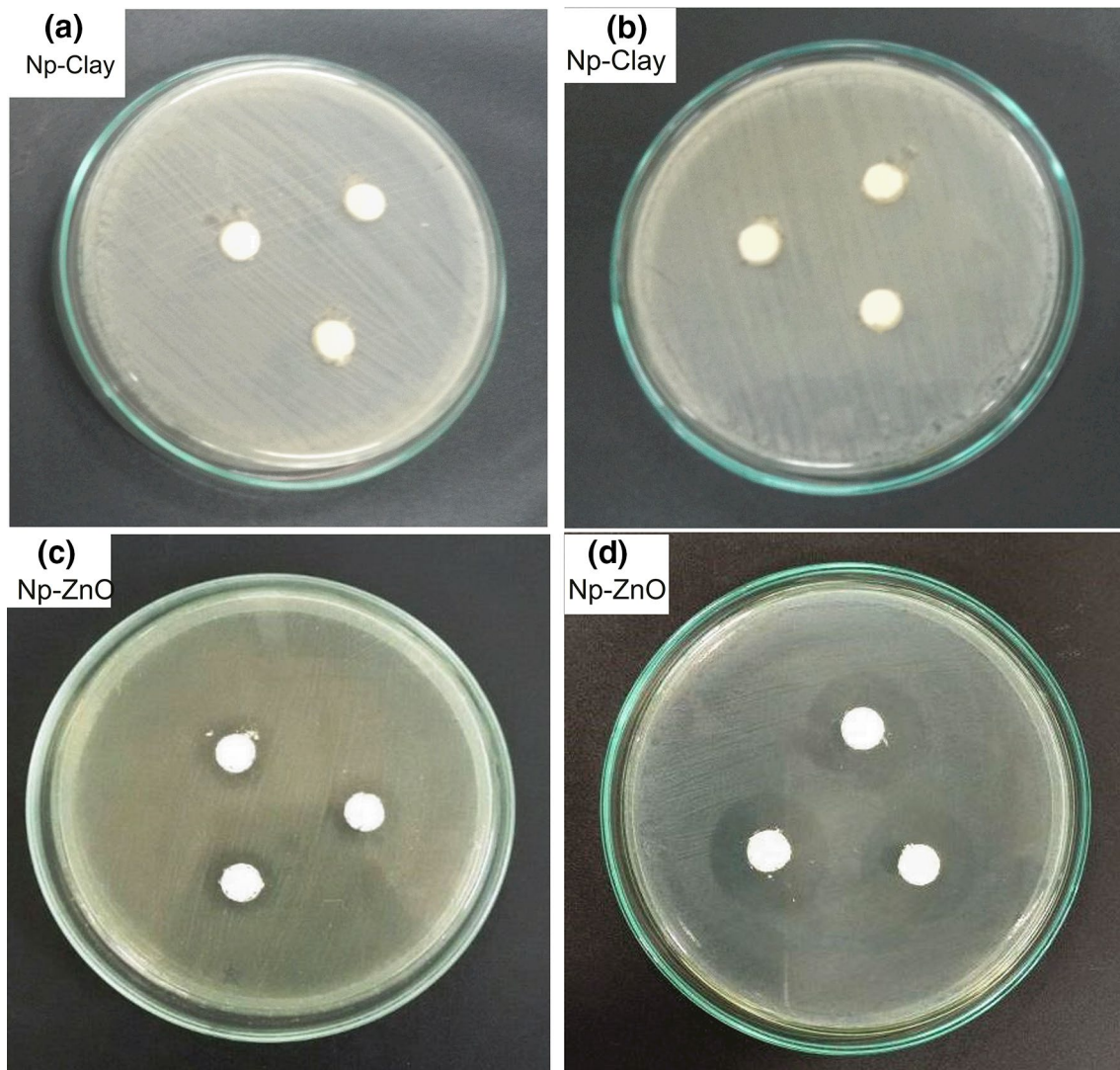
Fig. 13 Agar diffusion tests results on solid medium for Np-Clay: **a** *E. coli*; **b** *S. aureus*. Agar diffusion tests results on solid medium for Np-ZnO: **c** *E. coli*; **d** *S. aureus*

biopolymer (chitosan) has bacteriostatic activity, several authors [53, 54] claim that chitosan has antimicrobial potential. The results suggest that it is not occurring the migration of the active principle to the culture medium. For the chitosan sample containing organophilic clay (CClay) (Fig. 14) no inhibition halo was observed, suggesting that the organophilic clay used does not present bacteriostatic effect against the bacteria studied.

The samples CZnO, C4 and C9 (corresponding to Fig. 15) showed bacteriostatic effect for both bacteria due to the occurrence of an inhibition halo of microbial growth. It is possible to observe that the largest inhibition halos are observed to *S. aureus* gram-positive bacteria, because these bacteria have a ticker peptidoglycan cell wall, whereas *E. coli* the gram-negative bacteria have only one layer of
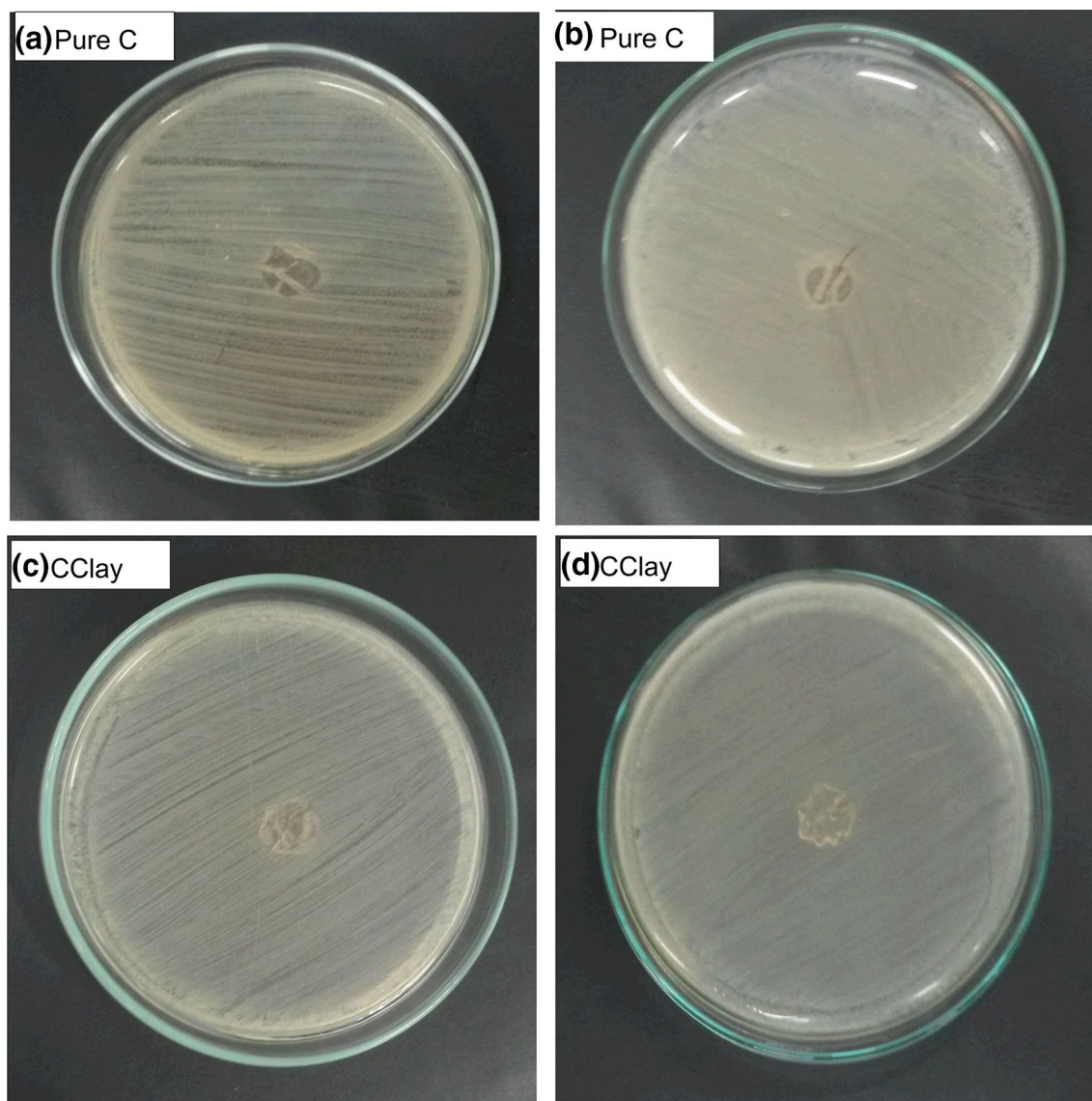
Fig. 14 Agar diffusion tests results for pure chitosan film (control): **a** *E. coli*; **b** *S. aureus*. Agar diffusion tests results for CClay: **c** *E. coli*; **d** *S. aureus*

lipopolysaccharide, but they have the advantage of being more resistant [55].

Figure 16 shows the microbiological results of death curve to *S. aureus* and *E. coli* bacteria, respectively, obtained for the nanocomposites films C, CClay, CZnO, C4 and C9. The results are expressed as bacterial colony amount per cm^2 of sample. As shown in Fig. 16a, all polymeric films showed antimicrobial activity against *S. aureus* bacteria. It is verified for a 6 h time contact, the samples presented a satisfactory antimicrobial activity. For pure chitosan sample (control) there was a reduction of 99.59%, for CClay 95.8%, CZnO 99.18%, C4 100% and C9 also 100%. Consequently, it is

observed that for a 24 h time the samples CClay and CZnO can reduce 100% of the microbial growth, except for pure chitosan sample (C) that maintains the same percentage as a 6 h time. It is interesting to mention that pure chitosan film presented antimicrobial potential, a fact that may be attributed to its strong interaction with the electronegative surface of the microorganisms, inducing changes in permeability, metabolic disorders and, finally, causing death [56]. Chitosan exhibits antimicrobial activity due to its cationic properties [57]. In addition, the amino group present in chitosan, when in acid medium, can be protonated to ammonium (NH_3^+), resulting in antifungal or antimicrobial activity [58]. It

Fig. 15 Agar diffusion tests results for CZnO: **a** *E. coli*; **b** *S. aureus*. Agar diffusion tests results for C4: **c** *E. coli*; **d** *S. aureus*. Agar diffusion tests results for C9: **e** *E. coli*; **f** *S. aureus*
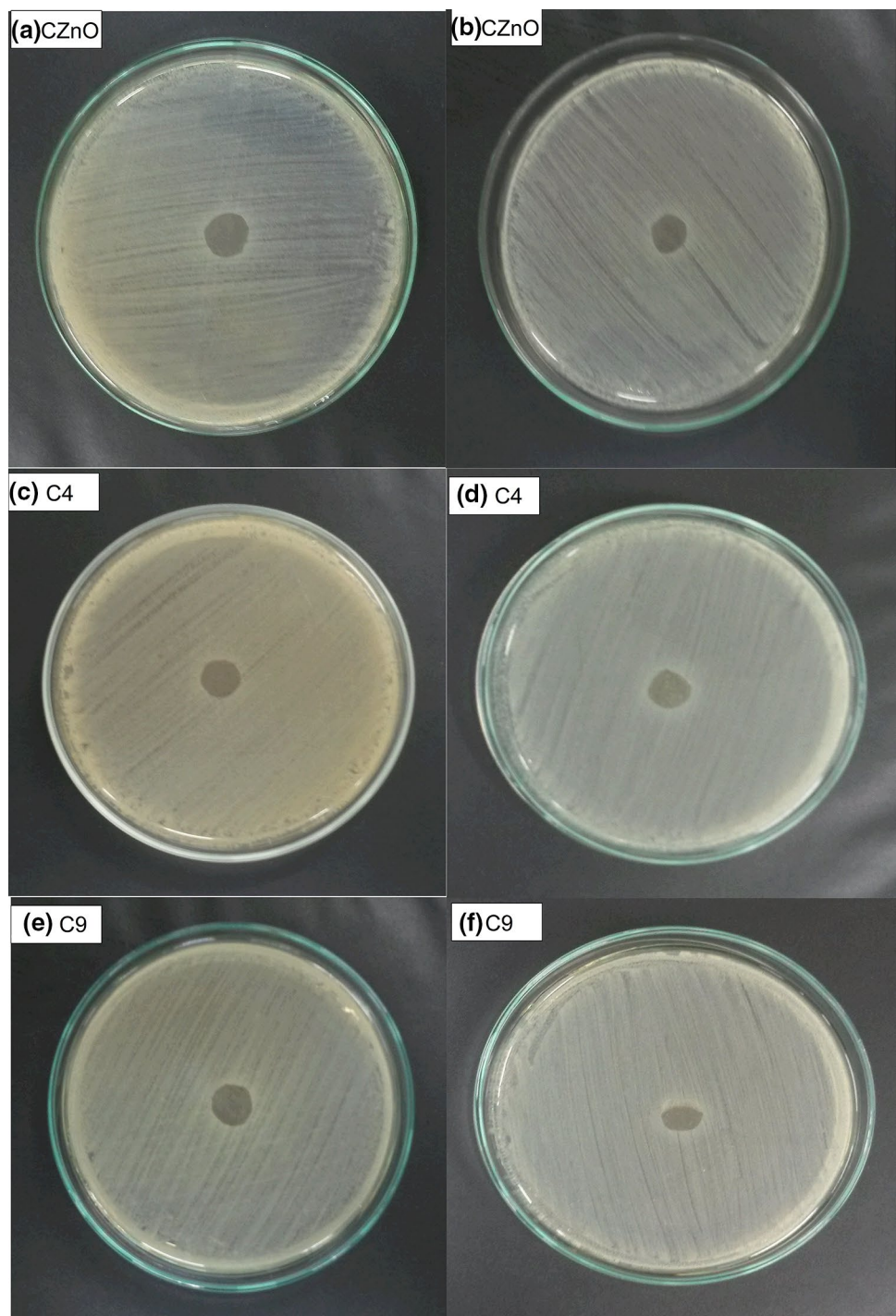
is also worth noting that the incorporation of an antimicrobial compound (ZnO) in a chitosan matrix improves this potential.

The antimicrobial activity of CClay sample may be correlated with the fact that a large amount of chitosan is used to produce the nanocomposites, which could increase its antimicrobial activity. In Fig. 16b there is a considerable drop in microbial growth for a 6 h time contact to *E. coli* bacteria. However, the only sample that can eliminate 100% of the bacteria is CZnO. The other samples follow with a reduction in the range of 91–95%. For a 24 h time contact, samples C4 and C9 failed to reduce 100% of the bacterial growth, suggesting that gram-negative bacteria exhibit a higher resistance, as mentioned before.

(a)

(b)
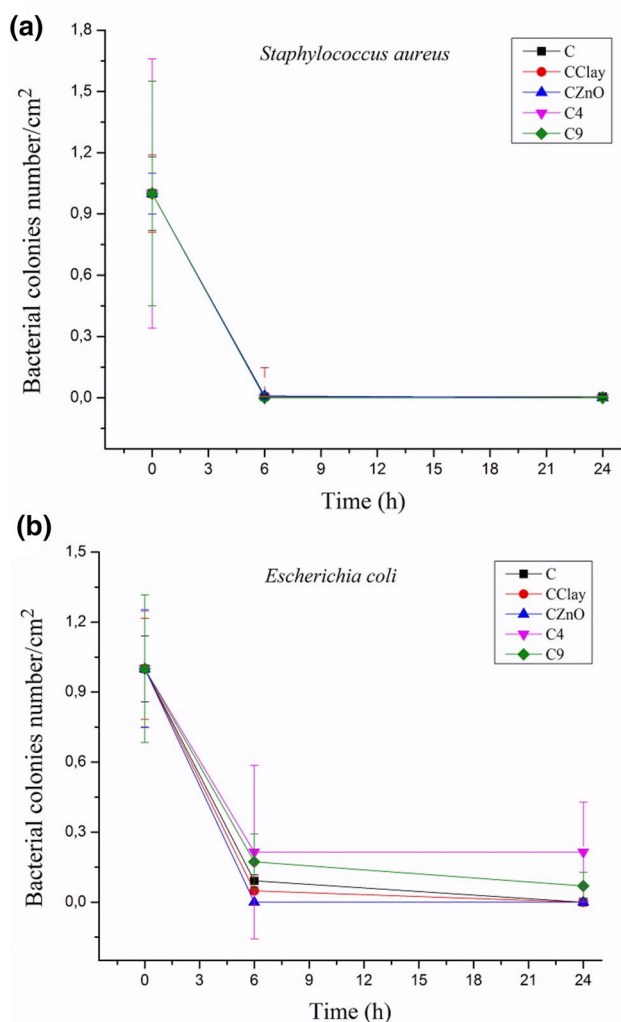
Fig. 16 Death *curve* for *S. aureus* (**a**) and *E. coli* (**b**) bacteria obtained with pure chitosan (C) films and incorporated with Np-A and Np-ZnO

Conclusions

In this investigation chitosan/ZnO nanoparticles/nano-organoclay nanocomposite were successfully prepared via polymer intercalation method by solution using acetic acid as solvent. Based on our research, the nano-organoclay compatibilized the chitosan and ZnO phases resulting in nanocomposite with enhanced physical and mechanical properties. The sample C4 (3% clay + 8% ZnO) had the best mechanical properties of tensile strength, elongation at break and Young's modulus. In addition, chitosan nanocomposites presented antimicrobial activity against *S. aureus* and *E. coli*. The analysis shows a synergistic effect of antimicrobial action only between chitosan and Np-ZnO. This effect was both bacteriostatic as bactericidal. Interestingly, nano-organoclay did not affected the antimicrobial activity of nanocomposite.

Based on the results of this research, the developed chitosan nanocomposite presented improved mechanical and antimicrobial properties, which makes it promising material for prospective application in food packaging production. However, studies with real food samples are still necessary to evaluate the effectiveness of the developed nanocomposite.

Compliance with Ethical Standards

Conflict of interest The authors declare that they have no conflicts of interest.

References

1. Yoo J, Irvine DJ, Discher DE, Mitragotri S (2011) Bio-inspired, bioengineered and biomimetic drug delivery carriers. Nat Rev Drug Discov 10:521–535
2. López-Mata MA, Ruiz-Cruz S, de Jesús O-P et al (2018) Mechanical, barrier and antioxidant properties of chitosan films incorporating cinnamaldehyde. J Polym Environ 26:452–461
3. Rani S, Kumar R (2019) A review on material and antimicrobial properties of soy protein isolate film. J Polym Environ 27:1613–1628
4. Gutiérrez TJ (2018) Active and intelligent films made from starchy sources/blackberry pulp. J Polym Environ 26:2374–2391
5. Giunchedi P, Genta I, Conti B et al (1998) Preparation and characterization of ampicillin loaded methylpyrrolidinone chitosan and chitosan microspheres. Biomaterials 19:157–161
6. Rinaudo M (2006) Chitin and chitosan: properties and applications. Prog Polym Sci 31:603–632
7. Leceta I, Guerrero P, de la Caba K (2013) Functional properties of chitosan-based films. Carbohydr Polym 93:339–346
8. Ounkaew A, Kasemsiri P, Kamwilaisak K et al (2018) Polyvinyl alcohol (PVA)/starch bioactive packaging film enriched with antioxidants from spent coffee ground and citric acid. J Polym Environ 26:3762–3772
9. Alabaraoye E, Achilonu M, Hester R (2018) Biopolymer (Chitin) from various marine seashell wastes: isolation and characterization. J Polym Environ 26:2207–2218
10. Atangana E, Chiweshe TT, Roberts H (2019) Modification of novel chitosan-starch cross-linked derivatives polymers: synthesis and characterization. J Polym Environ 27:979–995
11. Cagri A, Ustunol Z, Ryser E (2004) Antimicrobial edible films and coatings. J Food Prot 67:833–848
12. Wu C, Li Y, Du Y et al (2019) Preparation and characterization of konjac glucomannan-based bionanocomposite film for active food packaging. Food Hydrocolloids 89:682–690
13. Haghighi H, De Leo R, Bedin E et al (2019) Comparative analysis of blend and bilayer films based on chitosan and gelatin enriched with LAE (lauroyl arginate ethyl) with antimicrobial activity for food packaging applications. Food Packag Shelf Life 19:31–39
14. Abdel Ghaffar AM, Ali HE, Nasef SM, El-Bialy HA (2018) Effect of gamma radiation on the properties of crosslinked chitosan nano-composite film. J Polym Environ 26:3226–3236

15. de Oliveira ACS, Ugucioni JC, da Rocha RA et al (2019) Chitosan/polyaniline conductive blends for developing packaging: electrical, morphological, structural and thermal properties. J Polym Environ. 27:2250

16. Otsubo Y, Kato C (1954) Hydrothermal synthesis of montmorillonite type silicates. III. synthesis of zinc-montmorillonite. J Chem Soc Jpn 75:456–459

17. Al-naamani L, Dobretsov S, Dutta J (2016) Chitosan-zinc oxide nanoparticle composite coating for active food packaging applications. Innov Food Sci Emerg Technol 38:231–237

18. Cabuk M, Alan Y, Unal HI (2017) Enhanced electrokinetic properties and antimicrobial activities of biodegradable chitosan/organo-bentonite composites. Carbohydr Polym 161:71–81

19. Sanuja S, Agalya A, Umapathy MJ (2015) Synthesis and characterization of zinc oxide–neem oil–chitosan bionanocomposite for food packaging application. Int J Biol Macromol 74:76–84

20. Li L-H, Deng J-C, Deng H-R et al (2010) Synthesis and characterization of chitosan/ZnO nanoparticle composite membranes. Carbohydr Res 345:994–998

21. Salari M, Sowti Khiabani M, Rezaei Mokarram R et al (2018) Development and evaluation of chitosan based active nanocomposite films containing bacterial cellulose nanocrystals and silver nanoparticles. Food Hydrocolloids 84:414–423

22. Kumar S, Shukla A, Baul PP et al (2018) Biodegradable hybrid nanocomposites of chitosan/gelatin and silver nanoparticles for active food packaging applications. Food Packag Shelf Life 16:178–184

23. Abdollahi M, Rezaei M, Farzi G (2012) A novel active bionanocomposite film incorporating rosemary essential oil and nanoclay into chitosan. J Food Eng 111:343–350

24. Deng H, Lin P, Xin S et al (2012) Quaternized chitosan-layered silicate intercalated composites based nanofibrous mats and their antibacterial activity. Carbohydr Polym 89:307–313

25. Vlacha M, Giannakas A, Katapodis P et al (2016) On the efficiency of oleic acid as plasticizer of chitosan/clay nanocomposites and its role on thermo-mechanical, barrier and antimicrobial properties—comparison with glycerol. Food Hydrocolloids 57:10–19

26. Ambre AH, Katti KS, Katti DR (2010) Nanoclay Based composite scaffolds for bone tissue engineering applications. J Nanotechnol Eng Med 1:031013

27. Macuvele DLP, Colla G, Cesca K et al (2019) UHMWPE/HA biocomposite compatibilized by organophilic montmorillonite: An evaluation of the mechanical-tribological properties and its hemocompatibility and performance in simulated blood fluid. Mater Sci Eng C 100:411–423

28. Jiménez A, Roxana Ruseckaite RA (2012) Environmental silicate nano-biocomposites. Springer, Berlin, p 393

29. Rhim JW, Wang LF, Hong SI (2013) Preparation and characterization of agar/silver nanoparticles composite films with antimicrobial activity. Food Hydrocolloids 33:327–335

30. Souza VGL, Pires JRA, Vieira ÉT et al (2019) Activity of chitosan-montmorillonite bionanocomposites incorporated with rosemary essential oil: From in vitro assays to application in fresh poultry meat. Food Hydrocolloids 89:241–252

31. Qin Y, Liu Y, Yuan L et al (2019) Preparation and characterization of antioxidant, antimicrobial and pH-sensitive films based on chitosan, silver nanoparticles and purple corn extract. Food Hydrocolloids 96:102–111

32. Priyadarshi R, Negi YS (2017) Effect of varying filler concentration on zinc oxide nanoparticle embedded chitosan films as potential food packaging material. J Polym Environ 25:1087–1098

33. Blasco C, Picó Y (2011) Determining nanomaterials in food. TrAC, Trends Anal Chem 30:84–99

34. Katti KS, Katti DR, Dash R (2008) Synthesis and characterization of a novel chitosan/montmorillonite/ hydroxyapatite nanocomposite for bone tissue engineering. Biomed Mater 3:034122

35. Motshekga SC, Sinha S, Onyango MS, Momba MNB (2015) Preparation and antibacterial activity of chitosan-based nanocomposites containing bentonite-supported silver and zinc oxide nanoparticles for water disinfection. Appl Clay Sci 114:330–339

36. Müller L (2013) Incorporação de óleo essencial de cravo em membranas de quitosana e avaliação da atividade antimicrobiana e cicatrizante. Universidade Federal de Santa Catarina

37. Signini R, Campana Filho SP (1998) Purificação e caracterização de quitosana comercial. Polímeros 8:63–68

38. Massinga PH, Focke WW, de Vaal PL, Atanasova M (2010) Alkyl ammonium intercalation of Mozambican bentonite. Appl Clay Sci 49:142–148

39. Macuvele DLP, Nones J, Matsinhe JV et al (2017) Simultaneous effect of reaction temperature and concentration of surfactant in organo-bentonite synthesis. Mater Sci Forum 899:42–47

40. Siripatrawan U, Harte BR (2010) Physical properties and antioxidant activity of an active film from chitosan incorporated with green tea extract. Food Hydrocolloids 24:770–775

41. Brugnerotto J, Lizardi J, Goycoolea F et al (2001) An infrared investigation in relation with chitin and chitosan characterization. Polymer 42:3569–3580

42. Sanuja S, Agalya A, Umapathy MJ (2014) Studies on magnesium oxide reinforced chitosan bionanocomposite incorporated with clove oil for active food packaging application. Int J Polym Mater Polym Biomater. https://doi.org/10.1080/00914037.2013.879445

43. Wang X, Du Y, Yang J et al (2006) Preparation, characterization and antimicrobial activity of chitosan/layered silicate nanocomposites. Polymer 47:6738–6744

44. Szymanska E, Winnicka K (2015) Stability of chitosan- A challenge for pharmaceutical and biomedical applications. Marine Drugs 13:1819–1846

45. Kittur FS, Harish Prashanth KV, Udaya Sankar K, Tharanathan RN (2002) Characterization of chitin, chitosan and their carboxymethyl derivatives by differential scanning calorimetry. Carbohydr Polym 49:185–193

46. Martins CS, Morgado DL, Benedito O, Assis G (2016) Cashew gum-chitosan blended films:spectral, mechanical and surface wetting evaluations. Macromol Res 24:691–697

47. Ma X, Zhang W (2009) Effects of flower-like ZnO nanowhiskers on the mechanical, thermal and antibacterial properties of waterborne polyurethane. Polym Degrad Stab 94:1103–1109

48. Chrissafis K, Bikiaris D (2011) Can nanoparticles really enhance thermal stability of polymers? Part I: an overview on thermal decomposition of addition polymers. Thermochim Acta 523:1–24

49. Sakurai K, Maegawa T, Takahashi T (2000) Glass transition temperature of chitosan and miscibility of chitosan/poly(N-vinyl pyrrolidone) blends. Polymer 41:7051–7056

50. El-Hefian EA, Nasef MM, Yahaya AH (2011) Preparation and characterization of chitosan/poly(vinyl alcohol) blended films: Mechanical, thermal and surface investigations. E J Chem 8:91–96

51. Azizi S, Ahmad MB, Ibrahim NA et al (2014) Cellulose nanocrystals/ZnO as a bifunctional reinforcing nanocomposite for poly(vinyl alcohol)/chitosan blend films: fabrication, characterization and properties. Int J Mol Sci 15:11040–11053

52. da Silvano JR, Santa RAAB, Martins MAPM et al (2018) Nanocomposite of erucamide-clay applied for the control of friction coefficient in surfaces of LLDPE. Polym Test 67:1–6

53. Tianwei T, Xiaojing H, Weixia D (2001) Adsorption behaviour of metal ions on imprinted chitosan resin. J Chem Technol Biotechnol. https://doi.org/10.1002/jctb.358

54. Hu SG, Jou CH, Yang MC (2003) Protein adsorption, fibroblast activity and antibacterial properties of poly(3-hydroxybutyric acid-co-3-hydroxyvaleric acid) grafted with chitosan and chitooligosaccharide after immobilized with hyaluronic acid. Biomaterials 24:2685

55. Muñoz-Bonilla A, Fernández-García M (2012) Polymeric materials with antimicrobial activity. Prog Polym Sci 37:281–339

56. Shao WF, Chin FL, Daniel S (1994) Antifungal activity of chitosan and its preservative effect on low sugar candied Kumquat. J Food Prot 57:136–140

57. Han Y-S, Lee S-H, Choi KH, Park I (2010) Preparation and characterization of chitosan–clay nanocomposites with antimicrobial activity. J Phys Chem Solids 71:464–467

58. Jung B-O, Kim C-H, Choi K-S et al (1999) Preparation of amphiphilic chitosan and their antimicrobial activities. J Appl Polym Sci 72:1713–1719

Publisher's Note Springer Nature remains neutral with regard to jurisdictional claims in published maps and institutional affiliations.

Affiliations

Camila Rodrigues[1] · Josiane Maria Muneron de Mello[2,3] · Francieli Dalcanton[2] · Domingos Lusitâneo Pier Macuvele[1,4] · Natan Padoin[1] · Márcio Antônio Fiori[2,3] · Cíntia Soares[1] · Humberto Gracher Riella[1]

✉ Domingos Lusitâneo Pier Macuvele
  lusitaneom24@gmail.com

1 Graduate Program in Chemical Engineering, Universidade Federal de Santa Catarina (UFSC), Florianópolis, SC 88040-900, Brazil

2 Post Graduate Program in Technology and Management of the Innovation, Universidade Comunitária da Região de Chapecó (UNOCHAPECÓ), Chapecó, SC 89809-000, Brazil

3 Post Graduate Program in Environmental Science, Universidade Comunitária da Região de Chapecó (UNOCHAPECÓ), Chapecó, SC 89809-000, Brazil

4 Department of Natural Sciences and Mathematics, University of Rovuma (Extinct Universidade Pedagógica)-Extension of Niassa, Lichinga, Mozambique